Chapter 1

Title goes here

1.1 Introduction

TODO, pull from proposal and proposal-r1.

1.2 Methods

1.2.1 Participants

A total of 58 students from the University of Colorado Boulder participated in the experiment (ages 18-28 years, mean=21; 31 male, 27 female). EEG was recorded from 29 of the participants while they completed the experiment. The remaining 29 participants completed a solely behavioral experiment without EEG recording. All participants were right-handed and reported normal or corrected-to-normal vision. Participants either received course credit or payment of $15 per hour as compensation for their participation. Informed consent was obtained from each participant prior to the experiment in accordance with Institutional Review Board policy at the University of Colorado.

1.2.2   Stimuli

Novel "paper clip" objects similar to those used in previous studies (Bulthoff & Edelman, 1992; Edelman & Bulthoff, 1992; Logothetis, Pauls, Bulthoff, & Poggio, 1994; Logothetis, Pauls, & Poggio, 1995; Sinha & Poggio, 1996) were created using MATLAB. Eight vertices were placed randomly on the surface of a sphere of unit radius and then joined together with line segments. The last and first vertex were also joined to form a closed loop so that line segment terminations were not a salient feature (Balas & Sinha, 2009). Objects were constrained to exclude extremely acute angles between successive segments (less than 20 degrees) and were approximately rotationally balanced (center of mass within 10% of the origin). Objects were were rotated completely about their vertical axis in steps of 12 degrees and rendered to bitmap images under an orthographic projection. A total of 16 objects were created using this procedure, yielding 480 images (30 images per object). Object examples are shown in Figure 1.1.

1.2.3   Procedure

Participants observed an entraining sequence of rotated views of a random object and performed a same-different judgement about a probe stimulus. On each trial, a view was randomly selected as the initial view of the sequence followed by seven additional views spaced 24 degrees apart (Figure 1.2A, blue tick marks). Thus, the eight view entraining sequence spanned 168 degrees of the object. The entraining sequence was either presented in order (i.e., spatially predictable) or randomized. Following the entraining sequence after a 200 ms blank was a probe stimulus consisting of either an unseen view from the entraining object or a novel distractor. Unseen views were randomly sampled from the 12 degree interpolations between views of the entraining sequence (Figure 1.2A, magenta tick marks) and from outside of the span of the entraining sequence in increments of 24 degrees (Figure 1.2A, green tick marks).

Distractors were created from the original target objects by randomly selecting new spherical coordinates for six of the eight vertices and re-rendering them to bitmap images using the same

**A**

B

Figure 1.1: Novel "paper clip" objects

A: Objects were composed of eight three-dimensional vertices joined together with line segments. To render the objects to bitmap images, each object was rotated completely about its vertical axis in steps of 12 degrees and reduced to an orthographic projection. **B:** Four of the 16 objects used in the experiment.

method as the original target objects (12 degree steps about the vertical axis). Distractors conformed to the same constraints as the original target objects (no extremely acute angles, approximately rotationally balanced). Participants were instructed to respond "same" if they believed the probe depicted the same object as the entraining sequence or "different" if it depicted a distractor object. Participants received feedback after each trial according to whether their response was correct or incorrect.

During the entraining sequence, object views were presented for 50 ms at either 10 Hz (i.e., temporally predictable) or at a variable rate by manipulating the interstimulus interval (ISI) between subsequent views. Temporally predictable ISIs were 50 ms, totaling 350 ms across the entraining sequence. Variable ISIs were selected by randomly generating seven ISIs that also summed to 350 ms (Figure 1.2B). ISIs were in the range of 16.67 ms (minimum) to 216.67 ms

(maximum) in increments of 16.67 ms. Temporal unpredictability was maximized by generating 400 such ISI sequences, calculating the summed squared error (SSE) across subsequent ISIs in a sequence, and selecting the 100 sequences with the highest SSE for use during the experiment.

A
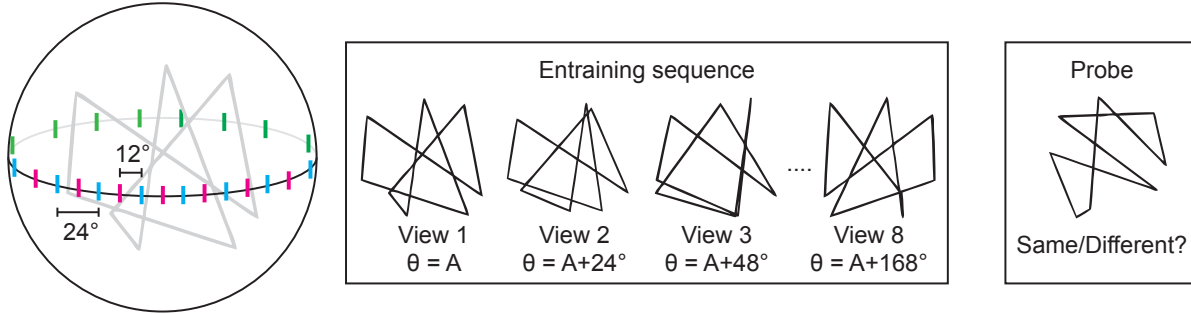
B **C**

Figure 1.2: Experimental procedure

A: Experimental trials contained an entraining sequence composed of eight views of a single object, followed by a probe stimulus. Entraining views were spaced 24 degrees apart (blue tick marks). The probe depicted an unseen view from the 12 degree interpolations between views of the entraining sequence (magenta tick marks) or from outside the span of the entraining sequence in increments of 24 degrees (green tick marks). **B:** Entraining views were either presented at 10 Hz with a 50 ms on time and 50 ms off time or in a temporally unpredictable manner with a 50 ms on time (gray segments) and variable off time (white segments). In both cases, the duration of the total entraining sequence was held constant at 750 ms. **C:** Order and timing of events within a single trial.

The experiment was displayed on an LCD monitor with a native resolution of 1280x1024 operating at 60 Hz using the Psychophysics Toolbox Version 3 (Brainard, 1997; Pelli, 1997). Stimuli

were presented on an isoluminant 50% gray background and subtended approximately 5 degrees of visual angle. Trials began with a fixation cross (200 ms) followed by a blank (400 ms), the entraining sequence (750 ms total), a second blank (200 ms), and ended with the probe stimulus (50 ms) (Figure 1.2C). Participants were required to respond within 2000 ms. Trials were separated by a variable intertrial interval of 2000-2400 ms. The experiment contained 500 trials with an additional 20 practice trials that contained a longer blank (1000 ms) between the entraining sequence and the probe to familiarize participants with the order of events during trials. Participants completed the 20 practice trials (which were discarded from analysis) prior to performing the 500 experimental trials.

1.2.4   EEG recording and preprocessing

The EEG was recorded using an Electrical Geodesics, Inc. (EGI) system composed of a 128 channel net (HCGSN 130) amplified through 200 MΩ amplifiers (Net Amps 200). The signal was sampled at 250 Hz with impedances for each electrode were adjusted to less than 40 kΩ before and during the recording. Stimulus and response trigger onsets were measured via the Psychophysics Toolbox using a high precision realtime clock that was synchronized within 2.5 ms of the EEG system's clock before every trial during the experiment.

EEG data were preprocessed using the FieldTrip toolbox (Oostenveld, Fries, Maris, & Schoffelen, 2011). Raw data were first band-pass filtered between 1 Hz and 100 Hz with a 59-61 Hz band-stop and then epoched into 2350 ms segments that spanned the start of the pre-trial blank to 1000 ms after the probe stimulus. Individual segments were visually inspected and rejected if found to contain muscle artifacts or atypical noise. Bad channels were also identified and temporarily removed from the data before performing ICA decomposition (Delorme & Makeig, 2004) to remove of ocular artifacts. Components related to ocular artifacts were identified based on their topographical distribution across electrodes. The data were reconstructed without the ocular components and any bad channels were replaced using spherical spline interpolation (Perrin, Pernier, Bertrand, & Echallier, 1989). The resulting segments were re-referenced to the average reference.

1.2.5   Event-related averaging

Event-related averaging was performed separately for the entraining sequence and the sub-sequent probe. For the entraining sequence, data were aligned to the onset of entraining views 2 through 8 and averaged from the period beginning 50 ms before each entrainer and ending 50 ms after. Baseline correction was performed using the first 50 ms of this period. For the probe, data were aligned to the probe onset and averaged from the period beginning 200 ms before the probe and ending 400 ms after. This allowed detection of predictability effects during the blank period due to differences in phase elicited by the entraining sequence as well as probe-evoked predictability effects.

All waveforms were averaged over a montage of 23 electrodes that covered the occipital and parietal cortices (Figure 1.3). The montage included locations from the 10-10 system that are commonly associated with perceptual processing (Oz, O1/O2, PO3/PO4, and PO7/PO8) (e.g., Doherty, Rao, Mesulam, & Nobre, 2005; Rohenkohl & Nobre, 2011; Fahrenfort, Scholte, & Lamme, 2007).
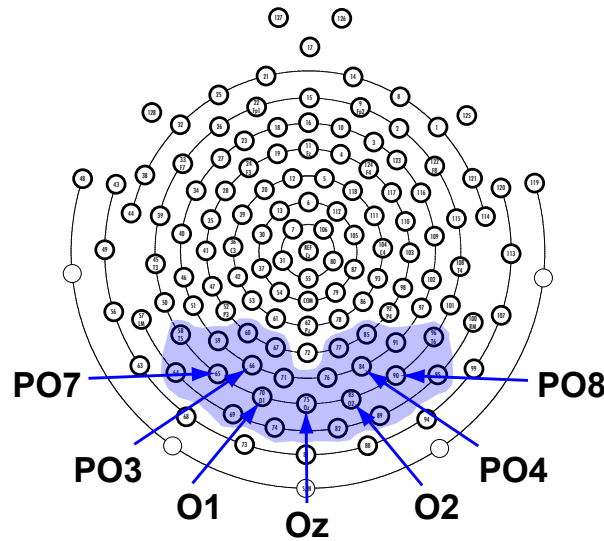

Figure 1.3: Electrode pooling for analyses

Blue shaded region denotes pooled electrodes. Locations from the 10-10 system are indicated.

1.2.6   Time-frequency analysis

Segmented data were used to compute time-frequency data for each trial. Data were first downsampled to 125 Hz and then used to compute the instantaneous Fourier coefficients at each time bin using a multi-taper approach. Hanning tapers were generated at 5-40 Hz and convolved with the data using a sliding time window (four cycles per frequency per time window). The relatively long time window required for low-frequency bands prevents computation of time-frequency data for short time segments, such as the 200 ms blank before the probe. To address this issue, time-frequency data was computed over the entire 2350 ms trial epoch and then cropped to investigate temporal regions of interest.

Power was computed from the magnitude of the instantaneous Fourier coefficients at each frequency (f) and time bin (t):

$$Power(f, t) = \frac{1}{n} \sum_{k=1}^{n} |F_k(f, t)|^2$$

Phase, which is normally defined as the angle of the complex Fourier coefficients, cannot be averaged due to its circularity and thus standard statistical models cannot be applied to assess its significance. One solution to this problem is to compute inter-trial coherence (ITC) instead (Lachaux, Rodriguez, Martinerie, & Varela, 1999). ITC is averaged in the complex domain by first normalizing phase information to unit length by dividing off power and computing the magnitude:

$$ITC(f, t) = \left| \frac{1}{n} \sum_{k=1}^{n} \frac{F_k(f, t)}{|F_k(f, t)|} \right|$$

ITC ranges between 0 and 1 and represents how systematic phase angles are across trials. A value of 0 indicates that phase information is essentially uniformly distributed across trials while a value of 1 indicates a high degree of phase-locking at a particular frequency across trials.

All time-frequency analyses were averaged over the same montage of 23 occipitoparietal electrodes that was used to compute event-related averages (Figure 1.3).

1.3   Results

1.3.1   Behavioral measures of spatial and temporal predictability

Five subjects were excluded from behavioral analysis for accuracy 2.7σ (or further) below mean accuracy across subjects. The remaining 53 subjects were submitted to a 2x2 ANOVA with spatial and temporal predictability as within-subjects factors. Experiment type (EEG or behavioral only) was included as an additional between-subjects factor to ensure that it did not interact with any of the within-subjects factors. Accuracy and reaction times were collected during the experiment and were used to compute *d'*, a measure of sensitivity that takes into account response bias, and inverse efficiency, a measure that combines accuracy and reaction times (Townshend & Ashby, 2005). These behavioral measures are plotted in Figure 1.4.

Subjects that completed the full EEG experiment were on average less accurate ($F(1, 51) = 4.80$, $p = 0.033$) but responded more quickly ($F(1, 51) = 10.05$, $p = 0.003$) than subjects that completed the solely behavioral experiment. These differences reflect a speed-accuracy tradeoff, likely due to differences in instructions given to subjects by experimenters or motivational differences between subject groups. Importantly, experiment type did not interact with any within-subjects factors (all *p*'s > 0.05) indicating that the behavioral measures of interest were not dependent on which type of experiment subjects completed.

Overall, subjects were more accurate when the entraining sequence was temporally predictable ($F(1, 51) = 17.84$, $p < 0.001$). A similar effect for spatial predictability failed to reach significance ($F(1, 51) = 1.85$, $p = 0.18$). The interaction between spatial and temporal predictability, however, was significant ($F(1, 51) = 6.13$, $p = 0.017$). LeabraTI as well as previous investigations of predictability (e.g., Doherty et al., 2005) suggest that spatial and temporal predictability should have an additive effect on behavioral outcomes. However, the combined spatial and temporal predictability condition here (denoted S+T+ in Figure 1.4) does not exhibit this pattern. Although not significantly different from spatial predictability alone ($t(52) = 1.29$, $p = 0.204$) or from temporal predictability alone ($t(52) = 0.45$, $p = 0.652$), this result merits further investigation.

Figure 1.4: Behavioral measures of spatial and temporal predictability

Accuracy, *d'* (sensitivity), reaction time, and inverse efficiency (reaction time divided by percent correct) as a function of entrainment condition. S-/+ refers to spatially unpredictable and predictable, T-/+ to temporally unpredictable and predictable. Error bars depict within-subjects error using the method described in Cousineau (2005) adapted for standard error.

When responses are transformed into *d'*, there is a significant effect of both spatial ($F(1, 51)$ = 4.71, p = 0.035) and temporal predictability ($F(1, 51)$ = 11.99, $p < 0.001$). This result suggests that response bias can partially explain why spatial predictability failed to reach significance for raw accuracy. Other potential reasons for this result are discussed later. The interaction between spatial and temporal predictability remained significant for *d'* ($F(1, 51)$ = 4.49, p = 0.039). The

interaction is additive, but is driven primarily by the strong effect of introducing spatial or temporal predictability over complete unpredictability (S-T- versus S+T-, $t(52) = 3.19$, $p = 0.002$; S-T- versus S+T+, $t(52) = 4.26$, $p < 0.001$) opposed to any synergistic effect of combined spatial and temporal predictability (S+T+ versus S+T-, $t(52) = 0.90$; S+T+ versus S-T+, $t(52) = 0.31$; both p's > 0.05).

Reaction times were significantly faster when the entraining sequence was temporally predictable ($F(1, 51) = 12.38$, $p < 0.001$). A similar effect for spatial predictability failed to reach significance ($F(1, 51) = 1.96$, $p = 0.168$) nor did the interaction term ($F(1, 51) = 0.05$, $p = 0.83$).

Inverse efficiency, which considers reaction time as a function of accuracy (defined as reaction time divided by percent correct) can be thought of as the amount of energy consumed by the system to produce a behavioral outcome (Townshend & Ashby, 1983). It is often used to remove non-monotonicities present in accuracy or reaction times alone, although that effect is not observed here. Nevertheless, it provides another lens under which to interpret the results, and thus it is considered here. Inverse efficiency was significantly lower when the entraining sequence was temporally predictable ($F(1, 51) = 23.31$, $p < 0.001$), but not when it was spatially predictability ($F(1, 51) = 0.002$, $p = 0.963$). Inverse efficiency is characterized by a significant cross-over interaction ($F(1, 51) = 5.85$, $p = 0.019$). Spatial predictability of the entraining sequence produces lowers inverse efficiency over complete unpredictability. Inverse efficiency is lowest on average when stimuli are temporally predictable, but the addition of spatial predictability causes an increase in inverse efficiency. These results suggest... **TODO**

1.3.2 Time course of spatial and temporal predictability

A total of five subjects were excluded from EEG analysis – three for an overabundance of artifacts in the EEG recording resulting in low trial counts after rejection and two for accuracy 2.7σ (or further) below mean accuracy across subjects (these two subjects were also excluded from behavioral analyses, see preceding section). The remaining 24 subjects were included in all EEG analyses.

A 2x2 ANOVA with spatial and temporal predictability as within-subjects factors was used

to assess statistical significance at each time bin of event-related averages. *p*-values were corrected for a maximum false discovery rate (FDR) of 5% using the method described in Benjamini and Yekutieli (2001). Additionally, effects were only considered significant if they persisted for at least 16 ms.

To investigate the build-up of spatial and temporal predictability over the entraining sequence, activity from the second through final entraining views was averaged for each condition (the first entraining view is unpredictable, so it is omitted from the average). The results of this analysis are plotted in Figure1.5. The first thing worth noting is that a large 10 Hz periodicity is present for the temporally predictable conditions (S-T+ and S+T+), phase aligned approximately to the onset of each entrainer. Temporally unpredictable entrainers (S-T- and S+T-) are also approximately periodic. The reason for the 10 Hz periodicity in these conditions despite being temporally unpredictable is likely due to the 750 ms constant duration of the entraining sequence regardless of condition (Figure 1.2B). Presenting eight stimuli in 750 ms with a variable ISI is a 10 Hz presentation rate on average. Still, the temporally unpredictable entrainers exhibit markedly weaker amplitude and are approximately 180 degrees out of phase with the the temporally predictable entrainers.

The effect of spatial predictability manifested 26 ms after the onset of the entrainer and persisted for at least another 24 ms (one quarter of the 10 Hz period). Temporal predictability, in contrast, manifested prior to (-38 through -22 ms pre-stimulus) and at the onset of the entrainer (-6 ms pre-stimulus through 18 ms post-stimulus). The effect of temporal predictability appears to be driven by the anti phase relationship between T- and T+ conditions at these time points. Together, these effects demonstrate differential time courses for spatial and temporal predictability. Spatial predictability is a post-stimulus process and might represent a comparison computation between the previous stimulus and the currently presented one. Temporal predictability, in contrast, is a truly anticipatory process, occurring before (and at) the onset of each stimulus.

Spatial predictability was enhanced when stimuli were temporally predictable. This effect is characterized by the significant interaction between spatial and temporal predictability starting 14
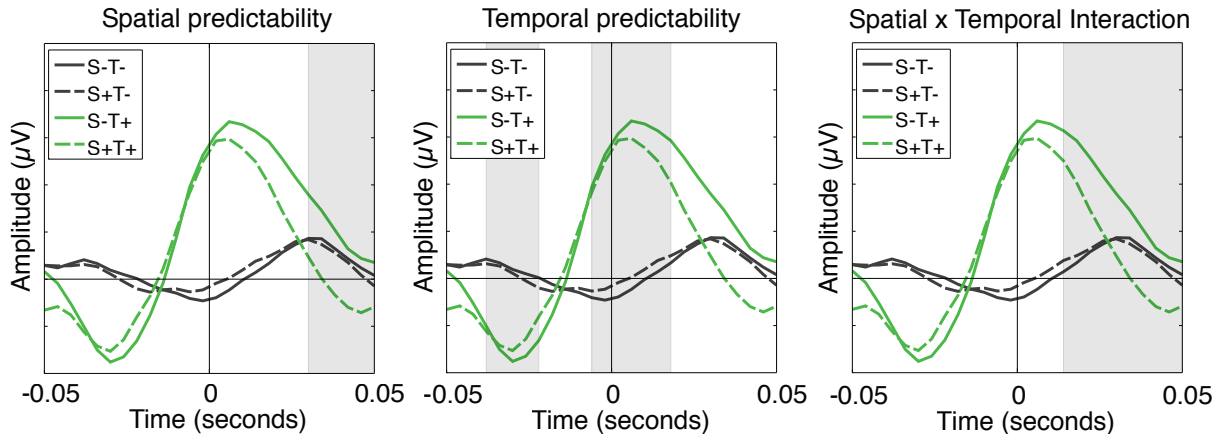
Figure 1.5: Entrainer-evoked activity

Grand averages for entrainers 2 through 8 as a function of entrainment condition. S-/+ refers to spatially unpredictable and predictable, T-/+ to temporally unpredictable and predictable. All plots depict the grand average with gray shaded regions denoting significant effects of spatial predictability (left), temporal predictability (center), and the interaction between these terms controlling for a maximum false discovery rate (FDR) of 5%.

ms after the onset of the entrainer and persisting for at least another 36 ms. This result indicates that the brain is more capable of differentiating between spatially coherent and random sequences of stimuli when it can properly anticipate the presentation of each stimulus (S-T+ versus S+T+) compared to when the onset is unpredictable.

To investigate the effect of spatial and temporal predictability on perception of the probe, waveforms were aligned to the probe onset onset averaged from 200 ms before through 400 ms after (Figure 1.6). The results of this analysis basically mirror the entrainer-evoked effects albeit with a few key differences. Temporal predictability was again a purely anticipatory process, manifesting within the pre-stimulus period (-184 ms through -160 ms and -132 ms through -108 ms pre-stimulus). Spatial predictability also manifested briefly within the pre-stimulus period (-128 ms through -80 ms pre-stimulus), which was not seen for spatially predictable entrainers. The post-stimulus effects of spatial predictability occurred much earlier than for entrainers and persisted much longer, beginning approximately at the onset of the probe (-12 ms pre-stimulus) and lasting 136 ms through the P1 response with several transient effects after.
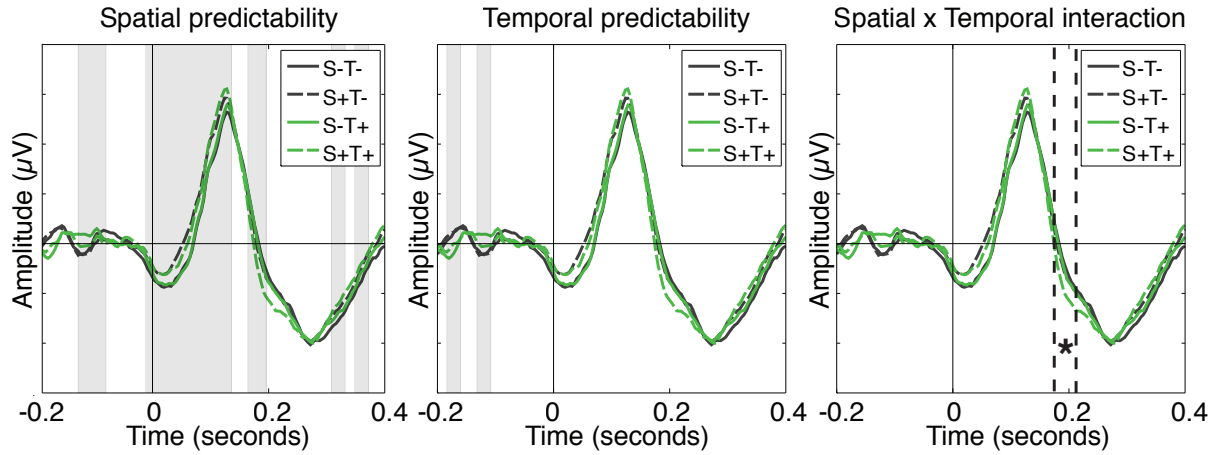
Figure 1.6: Probe-evoked activity

Grand averages for the probe stimulus, including the preceding 200 ms blank. S-/+ refers to spatially unpredictable and predictable, T-/+ to temporally unpredictable and predictable. All plots depict the grand average with gray shaded regions denoting significant effects of spatial predictability (left), temporal predictability (center), and the interaction between these terms controlling for a maximum false discovery rate (FDR) of 5%. The asterisk in the interaction plot denotes trending significance at the 5% level using amplitude averaged within the window defined by the dotted lines.

Unlike the significant interaction between spatial and temporal predictability for entrainers, the interaction for the probe failed to reach significance given the constraints of the statistical test (maximum FDR of 5%, 16 ms consecutive significance). However, averaging the amplitude within a window defined by exploratory analysis indicated a trending interaction from 170 ms to 210 ms ($F(1, 22) = 3.97$, $p = 0.059$). This effect is more pronounced and reaches significance if only the right hemisphere channels are considered ($F(1, 22) = 5.61$, $p = 0.027$), but fails to reach significance in the left hemisphere ($F(1, 22) = 2.24$, $p = 0.148$) explaining the trending effect when both hemispheres are considered jointly.

In summary, **TODO**

1.3.3   Predictability entrains alpha oscillations

The same 24 subjects used in event-related analyses (see preceding section) were used in time-frequency analyses described here. Statistical methods were also identical, consisting of a 2x2 ANOVA with spatial and temporal predictability as within-subjects factors and p-values were corrected for a 5% maximum FDR (Benjamini & Yekutieli, 2001). Effects were only considered significant if they persisted for at least 16 ms.

Power and inter-trial coherence (ITC), a measure of phase angle consistency across trials (Lachaux et al., 1999) were computed over a 5-20 Hz frequency range to investigate the relationship between entrainer predictability and alpha oscillatory properties (Figures 1.7-1.8). Both spatial and temporal predictability had a significant effect on 10 Hz power and ITC beginning around 200 ms after the onset of the first entrainer (power: 160-168 ms after entrainer 1; ITC: 136-208 ms after entrainer 1). This result indicates that 10 Hz entrainment takes around 2-3 events to establish, consistent with previous reports (Mathewson, Fabiani, Gratton, Beck, & Lleras, 2010). Spatial predictability had a suppressive effect on 10 Hz power and phase alignment whereas temporal predictability had a positive effect.

The effect of spatial predictability only persisted for three entrainers on average (duration ranges for 10 Hz power and ITC: 272-280 ms). Temporal predictability exhibited a sustained effect on 10 Hz power lasting nearly the entire entraining sequence. In the case of ITC, the effect of temporal predictability persisted throughout the blank period that separated the entraining sequence and the probe (Figure 1.9). This result indicates that alpha phase remained aligned even without exogenous entrainment. No alpha-band effects were significant during the actual presentation of the actual probe, however.

In summary, **TODO**

Figure 1.7: Effect of entrainer predictability on alpha power

Alpha-band power over the entraining sequence. The top row depicts main effects of spatial and temporal predictability on oscillatory power in the 5-20 Hz frequency range. The bottom row depicts 10 Hz only effects of spatial predictability (left), temporal predictability (center), and the interaction between these terms with gray shaded ranges indicating significance while controlling for a maximum false discovery rate (FDR) of 5%. Time axes indicate total trial time after the initial fixation cross with 0.4 seconds corresponding to the first entrainer.

1.3.4 Predictability effects in other oscillatory bands

The effects of spatial and temporal predictability on alpha oscillatory properties during the probe itself were investigated in other frequency bands to determine
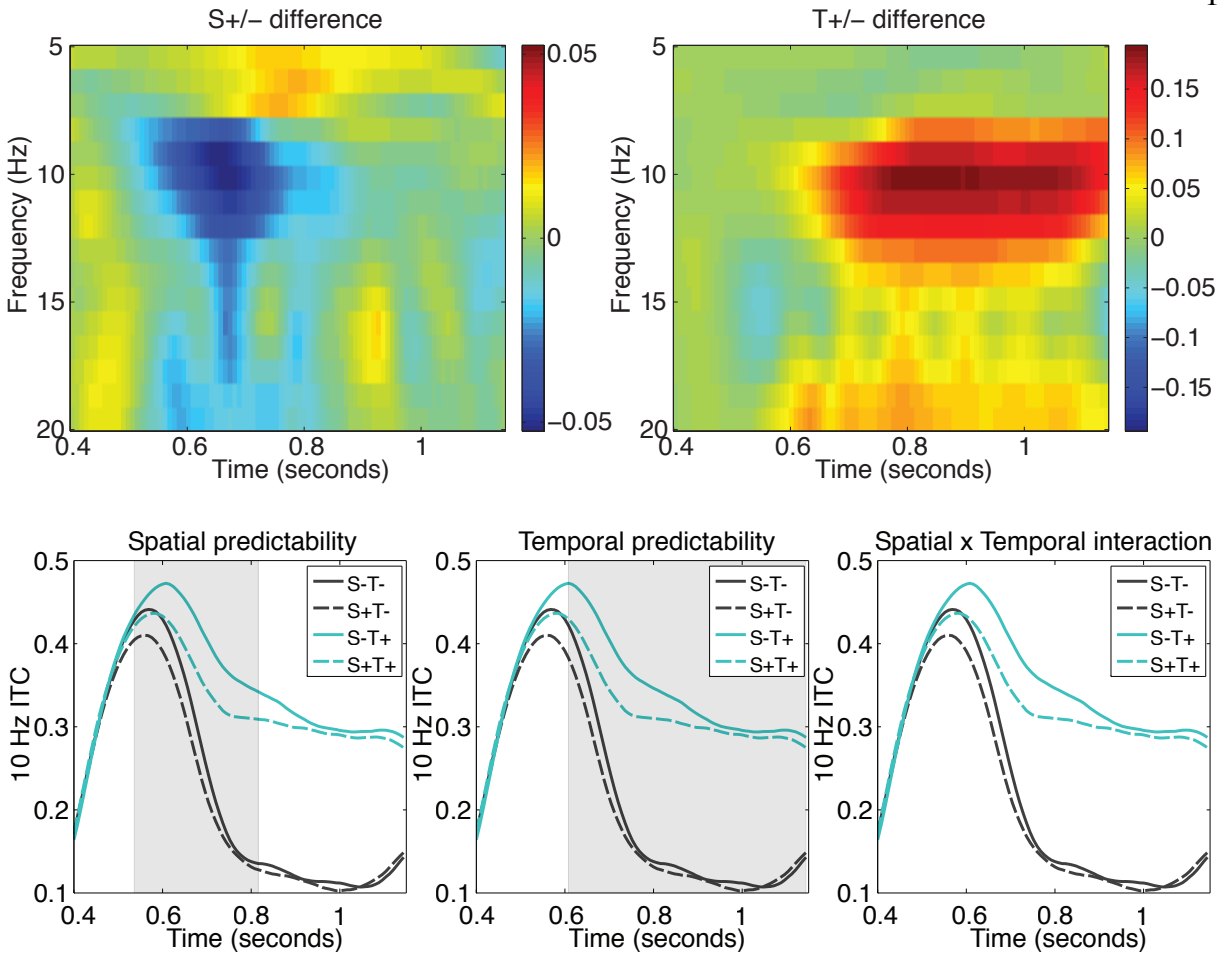
Figure 1.8: Effect of entrainer predictability on alpha phase coherence

Alpha-band inter-trial coherence (ITC) over the entraining sequence. The top row depicts main effects of spatial and temporal predictability on ITC coherence in 5-20 Hz frequency range. The bottom row depicts 10 Hz only effects of spatial predictability (left), temporal predictability (center), and the interaction between these terms with gray shaded ranges indicating significance while controlling for a maximum false discovery rate (FDR) of 5%. Time axes indicate total trial time after the initial fixation cross with 0.4 seconds corresponding to the first entrainer.

1.4   Discussion

References

Balas, B. J., & Sinha, P. (2009). The role of sequence order in determining view canonicality for novel wire-frame objects. Attention, Perception & Psychophysics, 71(4), 712–723.

Benjamini, Y., & Yekutieli, D. (2001). The control of the false discovery rate in multiple testing
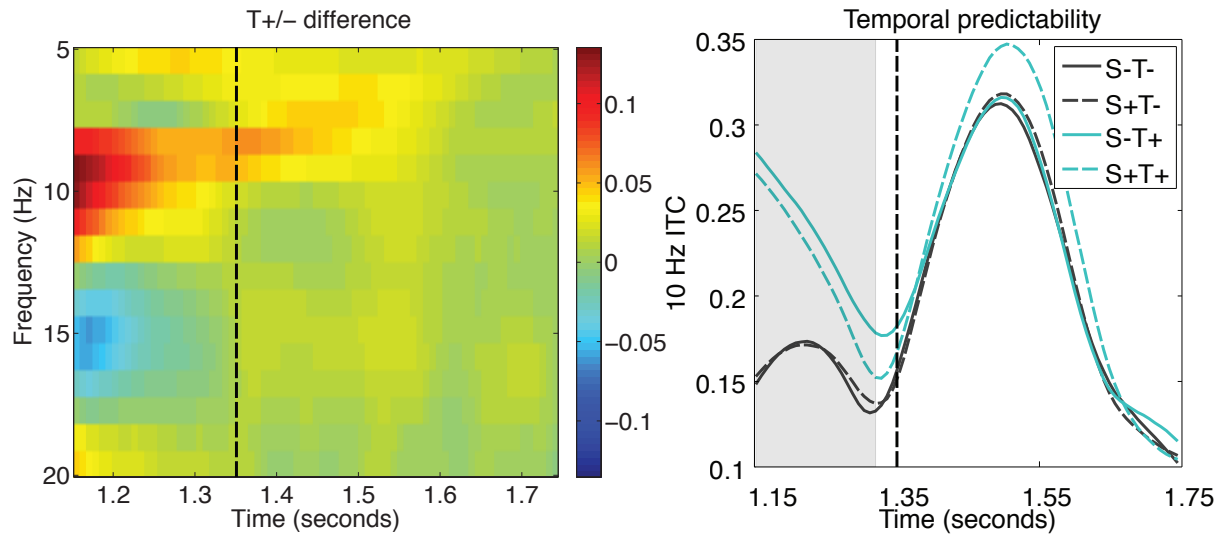
Figure 1.9: Alpha phase coherence before and after probe

Alpha-band inter-trial coherence (ITC) 200 ms preceding the probe and 400 ms following. Dotted vertical line indicates probe onset. Gray shaded ranges indicating significance while controlling for a maximum false discovery rate (FDR) of 5%. Time axes indicate total trial time after the initial fixation cross.

under dependency. The Annals of Statistics, 29(4), 1165–1188.

Brainard, D. (1997). The Psychophysics Toolbox. Spatial Vision, 10(4), 433–436.

Bulthoff, H. H., & Edelman, S. (1992). Psychophysical support for a two-dimensional view interpolation theory of object recognition. Proceedings of the National Academy of Sciences of the United States of America, 89(1), 60–64.

Cousineau, D. (2005). Confidence intervals in within-subject designs: A simpler solution to Loftus and Massons method. Tutorials in Quantitative Methods for Psychology, 1(1), 42–45.

Delorme, A., & Makeig, S. (2004). EEGLAB: An open source toolbox for analysis of single-trial EEG dynamics including independent component analysis. Journal of Neuroscience Methods, 134(1), 9–21.

Doherty, J. R., Rao, A., Mesulam, M. M., & Nobre, A. C. (2005). Synergistic effect of combined temporal and spatial expectations on visual attention. The Journal of Neuroscience, 25(36), 8259–8266.

Edelman, S., & Bulthoff, H. H. (1992). Orientation dependence in the recognition of familiar and novel views of three-dimensional objects. Vision Research, 32(12), 2385–2400.

Fahrenfort, J. J., Scholte, H. S., & Lamme, V. A. F. (2007). Masking disrupts reentrant processing in human visual cortex. Journal of Cognitive Neuroscience, 19(9), 1488–1497.

Lachaux, J. P., Rodriguez, E., Martinerie, J., & Varela, F. J. (1999). Measuring phase synchrony in brain signals. Human Brain Mapping, 8(4), 194–208.

Logothetis, N., Pauls, J., Bulthoff, H., & Poggio, T. (1994). View-dependent object recognition by monkeys. Current Biology, 4(5), 401–414.

Logothetis, N. K., Pauls, J., & Poggio, T. (1995). Shape representation in the inferior temporal cortex of monkeys. Current Biology, 5(5), 552–563.

Mathewson, K. E., Fabiani, M., Gratton, G., Beck, D. M., & Lleras, A. (2010). Rescuing stimuli from invisibility: Inducing a momentary release from visual masking with pre-target entrainment. Cognition, 115(1), 186–191.

Oostenveld, R., Fries, P., Maris, E., & Schoffelen, J.-M. (2011). FieldTrip: Open source software for advanced analysis of MEG, EEG, and invasive electrophysiological data. Computational Intelligence and Neuroscience, 2011.

Pelli, D. (1997). The VideoToolbox software for visual psychophysics: Transforming numbers into movies. Spatial Vision, 10(4), 437–442.

Perrin, F., Pernier, J., Bertrand, O., & Echallier, J. F. (1989). Spherical splines for scalp potential and current density mapping. Electroencephalography and Clinical Neurophysiology, 72(2), 184–187.

Rohenkohl, G., & Nobre, A. C. (2011). Alpha oscillations related to anticipatory attention follow temporal expectations. The Journal of Neuroscience, 31(40), 14076–14084.

Sinha, P., & Poggio, T. (1996). Role of learning in three-dimensional form perception. Nature, 384(6608), 460–463.

Townshend, J. T., & Ashby, F. G. (1983). Stochastic Modeling of Elementary Psychological Processes. Cambridge: Cambridge University Press.

Townshend, J. T., & Ashby, F. G. (2005). Methods of modeling capacity in simple processing systems. In J. N. Castellan Jr., & F. Restle (Eds.), Cognitive Theory: Volume 3 (pp. 200–239). Hillsdale, NJ: Lawrence Erlbaum Associates.